20th Australasian Fluid Mechanics Conference
Perth, Australia
5-8 December 2016

# Potential Energy in Vertical Natural Convection

**C. S. Ng, A. Ooi and D. Chung**

Department of Mechanical Engineering, The University of Melbourne, Melbourne, Victoria 3010, Australia

### Abstract

We study the role of potential energy using the mechanical energy framework for vertical natural convection (VC), which is a buoyancy driven flow between differentially heated vertical walls. The Rayleigh numbers range from $10^5$ to $10^9$ and the Prandtl number is set at 0.709. Guided by the framework for VC, we compare the rate of conversion from potential energy to kinetic energy with that for Rayleigh–Bénard convection (RBC). The rate of conversion driven by vertical buoyancy flux are comparable for both VC and RBC at matched Rayleigh numbers. However, the turbulent production rate as well as turbulent dissipation rate are higher for VC than for RBC at matched Rayleigh numbers, which suggest that small-scale turbulence is generated at much lower Rayleigh numbers in VC compared to RBC. In addition, the dissipation rate of kinetic energy in VC is directly proportional to the rate at which potential energy is available for conversion. This relationship is consistent with the values of mixing efficiency for VC (proportion of kinetic energy consumed by irreversible mixing), which is approximately 0.53 for the present Rayleigh number range. This value of mixing efficiency in VC is also close to the expected value of mixing efficiency in RBC, which is 0.5.

### Introduction

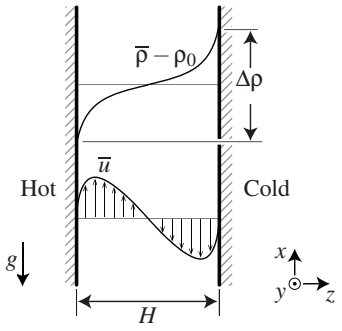


Figure 1: Setup of VC. $\overline{u}$ is the mean streamwise velocity, $\overline{\rho}$ is the mean density, $\rho_0$ is the reference density and $\Delta\rho$ is the density difference at the hot and cold walls. Gravity $g$ acts in the $-x$-direction.

We investigate the role of available potential energy and irreversible mixing in vertical natural convection (VC), see figure 1, which is a buoyancy driven flow between differentially heated vertical walls [7]. We consider the mechanical energy framework as proposed by Winters *et al.* [10], which distinguishes between the potential energy that is available for conversion into kinetic energy and the potential energy that is unavailable for conversion into kinetic energy, the former called the available potential energy and the latter called the background potential energy. Similar to Rayleigh–Bénard convection (RBC) [4], where heating is supplied at the bottom and removed from the top of a cell [1], and horizontal convection (HC) [2], where heat is supplied and removed through the bottom of a horizontal fluid layer [5], VC is a flow that is driven by potential energy alone.

### Flow Setup

We employ the same numerical setup for VC as in [7], i.e. we consider a buoyancy driven flow confined between two differentially heated walls. The governing continuity, momentum and temperature equations are respectively given by,

$$\partial_i u_i = 0, \tag{1}$$

$$\partial_t u_i + u_j \partial_j u_i = -\frac{1}{\rho_0}\partial_i p + \delta_{i1} g\beta(\Theta - \Theta_0) + \nu\partial_j^2 u_i, \tag{2}$$

$$\partial_t \Theta + u_j \partial_j \Theta = \kappa\partial_j^2 \Theta, \tag{3}$$

where $\partial_t \equiv \partial/\partial t$, $\partial_i \equiv \partial/\partial x_i$, $(i, j = 1, 2, 3)$ and repeated indices imply summation. We define $\Theta_0$ the reference temperature, $\beta$ the thermal expansion coefficient of the fluid, $\nu$ the kinematic viscosity and $\kappa$ the thermal diffusivity, all assumed to be independent of temperature. We also define the Rayleigh number $Ra \equiv g\beta\Delta\Theta H^3/(\nu\kappa)$, where $\Delta\Theta$ the temperature difference of the walls and the Prandtl number $Pr \equiv \nu/\kappa$. We further assume $(\rho - \rho_0)/\rho_0 = -\beta(\Theta - \Theta_0)$ the equation of state for gases and so we rewrite equations (2) and (3) as

$$\partial_t u_i + u_j \partial_j u_i = -\frac{1}{\rho_0}\partial_i p - \delta_{i1} g\frac{\rho}{\rho_0} + \nu\partial_j^2 u_i, \tag{4}$$

$$\partial_t \rho + u_j \partial_j \rho = \kappa\partial_j^2 \rho. \tag{5}$$

We will make use of equations (4) and (5), expressed in terms of density, in order to analyse the rate of conversions of potential energy to kinetic energy using the mechanical energy exchange framework for VC [10]. The coordinate system $x$, $y$ and $z$ (or $x_1$, $x_2$ and $x_3$) refers to the streamwise (opposing gravity), spanwise and wall-normal directions. We impose no-slip and no-penetration boundary conditions on $u_i$ at the walls, and periodic boundary conditions on $u_i$, $p$ and $\rho$ in the $x$- and $y$-directions. In addition, we adopt the notation $\langle\cdot\rangle_V$ for volume-averaged quantities, as before, and $\overline{(\cdot)}$ for time- and volume-averaged quantities. Thus, $\overline{u_i} = u_i - u_i'$ the mean velocity and $\overline{\rho} = \rho - \rho'$ the mean density. Equations (1), (4) and (5) are solved using DNS in a domain size $L_x \times L_y \times L_z = 8H \times 4H \times H$ and the simulation parameters have been previously reported in [7].

### Potential and Kinetic Energies in VC

One of the key ideas that characterises the contributions of potential energy to kinetic energy is the decomposition of potential energy $E_p$ into the available and background components ($E_a$ and $E_b$ respectively) [6]. $E_a$ is needed in order to drive natural convection and is the fraction of potential energy that can be converted to kinetic energy. $E_a$ is defined as the difference between $E_p$ the potential energy of a given density distribution and $E_b$ the potential energy of the background (reference) state of the density distribution in question [6], at that instant in time.

To determine the background state of an instantaneous density distribution in VC, we rearrange volumes of constant density such that lighter volumes are placed on top of heavier volumes. In a numerical simulation, a grid box of constant density is reshaped into a horizontal thin sheet and placed in the domain such that density reduces with increasing height [8]. The new

$x$-location of each value of density is denoted by $x_* = x_*(\rho,t)$. As an example, we plot the time-averaged profiles of $x_*$, i.e. $\langle x_* \rangle_t$ (where $\langle\cdot\rangle_t$ denotes averaging over time) versus density in figure 2 for $Ra$ ranging between $10^5$ to $10^9$ and $Pr = 0.709$. At the highest $Ra$, the thermal boundary layers are thinnest and so the density distribution is more uniform and closer to $\rho_0$, as reflected by the rapid change of $x_*/H$ at $|(\rho-\rho_0)/\Delta\rho| \lesssim 0.1$.

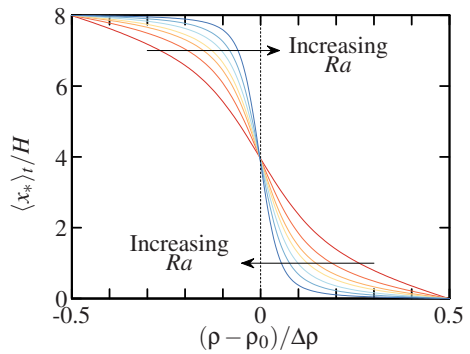


Figure 2: Time-averaged profiles of $\langle x_* \rangle_t / H$ of the density fields $(\rho-\rho_0)/\Delta\rho$ in VC. The density fields are rearranged such that lighter volumes are placed on top of heavier volumes.

Instantaneously, the background potential energy is then defined by $E_b \equiv g\langle(\rho-\rho_0)x_*\rangle_V/\rho_0$, where $g$ the gravitational acceleration and $\langle\cdot\rangle_V$ denotes averaging over the domain. In contrast, $E_p$ can be easily computed according to $E_p \equiv g\langle(\rho-\rho_0)x\rangle_V/\rho_0$ where $x$ is the original height of each volume of density in the domain. It then follows that $E_a = E_p - E_b$.

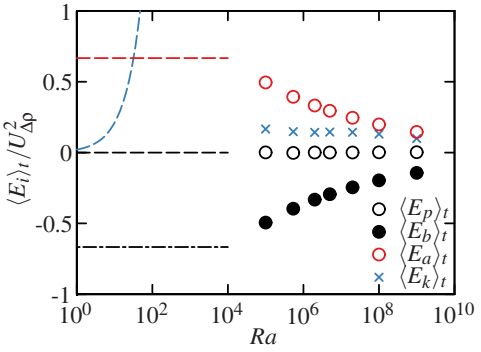


Figure 3: Mechanical energy distribution in VC, where $\langle E_p \rangle_t$ is the potential energy, $\langle E_b \rangle_t$ is the background potential energy, $\langle E_a \rangle_t = \langle E_p \rangle_t - \langle E_b \rangle_t$ is the available potential energy and $\langle E_k \rangle_t$ is the kinetic energy. The corresponding laminar solutions are shown as black dashes, black dot-dashes, red dashes and blue dashes. $U_{\Delta\rho} \equiv (g\Delta\rho H/\rho_0)^{1/2}$ is the free-fall velocity.

In figure 3, we plot the trends of $\langle E_p \rangle_t$, $\langle E_b \rangle_t$ and $\langle E_a \rangle_t$ for our VC dataset. $\langle E_p \rangle_t$ is equal to zero for our setup because we have set $\rho_0 = 0$ in our direct numerical simulations (DNS). The value for $\rho_0$ can be arbitrary since it only results in a vertical shift in the values of $\langle E_p \rangle_t$ and $\langle E_b \rangle_t$; the magnitude of $\langle E_a \rangle_t$ is unaffected. From figure 3, the values of $\langle E_b \rangle_t$ is always lower than $\langle E_p \rangle_t$ – this is expected since $\langle E_b \rangle_t$ represents the average minimum potential energy. In addition to potential energy, we compute $\langle E_k \rangle_t \equiv \langle u_i^2 \rangle_{V,t}/2$ the kinetic energy for VC, where $u_i$ the velocity field, and we find that $\langle E_k \rangle_t$ is smaller than $\langle E_a \rangle_t$ for the present $Ra$ range. For comparison, we include the laminar potential and kinetic energies which we compute from $\overline{u}(4\rho_0 H\nu) = \Delta\rho\, g(2z-H)(z-H)z$ the mean streamwise velocity and $2H(\overline{\rho}-\rho_0) = 2\Delta\rho z - \Delta\rho H$ the mean density equations. The laminar results are shown as dashed and dot-dashed curves in figure 3. Since we do not expect to extrapolate the laminar results to the turbulent regime, there are discontinuities in the laminar-to-turbulent trends. The trends at the lowest $Ra$ range in the laminar curves are consistent with the lower-$Ra$ trends of the DNS.

### Rate of Change of Kinetic and Potential Energies

Global form

We first derive the rate of change of kinetic energy ($\mathrm{d}E_k/\mathrm{d}t$) and potential energy ($\mathrm{d}E_p/\mathrm{d}t$). Following [10], we obtain

$$\frac{\mathrm{d}E_k}{\mathrm{d}t} = -\Phi_x + \Phi_\tau - \varepsilon, \tag{6}$$

by multiplying equation (4) with $u_i$ and then applying volume averaging. In a similar manner, we obtain

$$\frac{\mathrm{d}E_p}{\mathrm{d}t} = \Phi_{a1} + \Phi_x + \Phi_{b1} + \Phi_i, \tag{7}$$

by multiplying equation (5) with $x$ (i.e. potential energy varies linearly with vertical height) and then applying volume averaging. To facilitate discussion, we adopt the notation used by [10] for the terms in equations (6) and (7), where

$$\Phi_x = g\rho_0^{-1}\langle\rho u\rangle_V, \tag{8}$$

$$\Phi_\tau = \nu V^{-1}\oint_S (u_i\partial_j u_i)\cdot\hat{n}_j\,\mathrm{d}S \quad (=0), \tag{9}$$

$$\varepsilon = \nu\langle(\partial_j u_i)^2\rangle_V, \tag{10}$$

$$\Phi_{a1} = -g(\rho_0 V)^{-1}\oint_S (\rho x u_i)\cdot\hat{\mathbf{n}}\,\mathrm{d}S \quad \left(=-g\rho_0^{-1}\langle\rho U\rangle_{A(L_x,y,z)}\right), \tag{11}$$

$$\Phi_{b1} = \kappa g(\rho_0 V)^{-1}\oint_S (x\partial_i\rho)\cdot\hat{\mathbf{n}}\,\mathrm{d}S \quad (=0), \tag{12}$$

$$\Phi_i = -\kappa g\Delta\langle\rho\rangle_A(\rho_0 L_x)^{-1} \quad (=0), \tag{13}$$

and the notation $\langle\cdot\rangle_{A(L_x,y,z)}$ denotes averaging in the $yz$-plane at $x = L_x$. Where applicable, we include the simplified terms on the right-hand side (in parentheses) which we obtain from applying the boundary conditions of our VC setup. A similar set of equations to equations (6) and (7) has been previously developed by [4] for RBC. Equation (6) shows that the rate of change of $E_k$ depends on $\Phi_x$ the average buoyancy production rate in the domain, $\Phi_\tau$ the rate of work by shear stresses at the domain boundaries and $\varepsilon$ the average rate of dissipation of kinetic energy. In equation (7), the first term $\Phi_{a1}$ is the rate of buoyancy production at the upper boundary of the VC setup. The terms $\Phi_{b1}$ and $\Phi_i$ are relevant in setups that contain horizontal boundaries with a prescribed heat flux (in RBC, for example), the former is related to the heat flux rate at upper and lower horizontal boundaries and the latter is related to the conductive heat flux rate arising from a large scale vertical density difference if the flow is motionless. If our VC setup is instead adiabatically capped at the upper and lower boundaries, $\Phi_{a1}$ equals zero because the buoyancy production are suppressed at the boundaries, whereas $\Phi_{b1}$ remains zero (because there is no vertical heat flux at the boundaries) and $\Phi_i$ becomes finite. In our setup, $\Phi_\tau$, $\Phi_{b1}$ and $\Phi_i$ are equal to zero because (*i*) we impose no-slip and impermeable boundary conditions on $u_i$ in the $z$-direction, and (*ii*) we impose periodicity in the $x$- and $y$-directions. Thus, equation (6) is simplified to $\mathrm{d}E_k/\mathrm{d}t = -\Phi_x - \varepsilon$ and is the same as the equation for the conversion rate of $E_k$ of RBC [4], whereas equation (7) is simplified to $\mathrm{d}E_p/\mathrm{d}t = \Phi_{a1} + \Phi_x$.

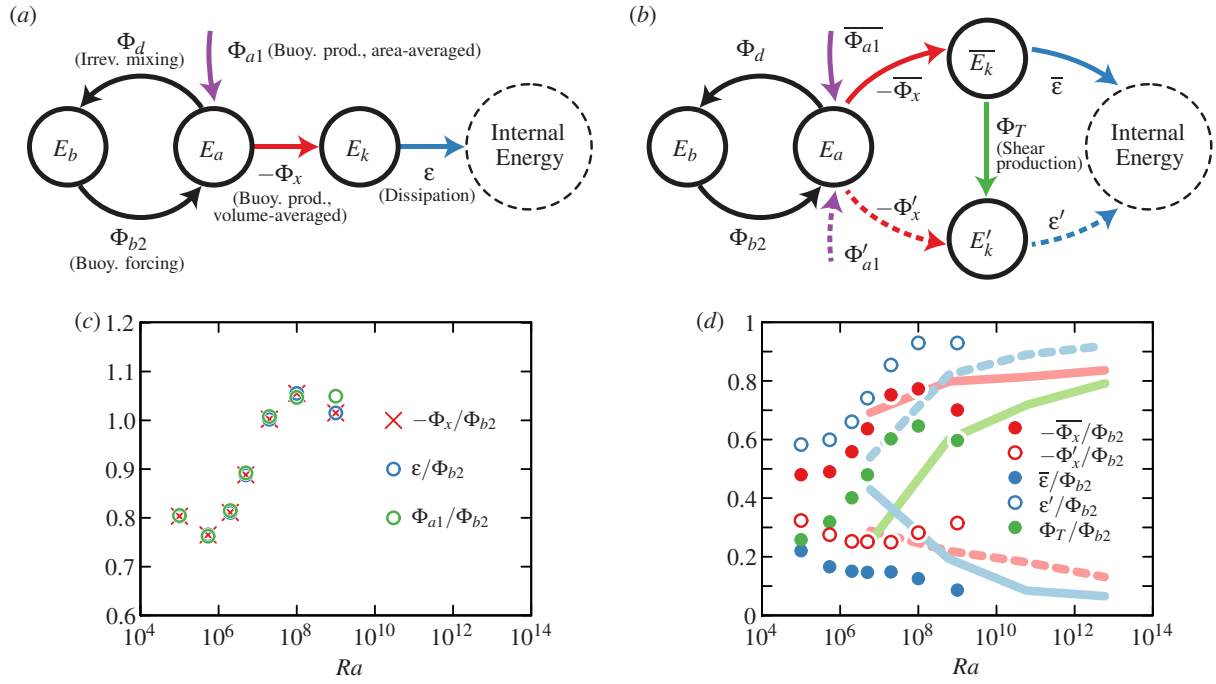


Figure 4: Mechanical energy framework for VC showing the pathways (arrows) for energy conversion rates between $E_b$ the minimum potential energy, $E_a$ the available potential energy and $E_k$ the kinetic energy. (*a*) Framework based on global volume-average equations (6), (14) and (17). (*b*) Framework based on the mean and turbulent contributions from equations (18)–(20). (*c*) *Ra* trends of the conversion rates in VC for volume-averaged buoyancy flux $\Phi_x$ (red crosses), dissipation $\varepsilon$ (blue circles) and area-averaged buoyancy production $\Phi_{a1}$ (green circles). For $\Phi_x$ and $\varepsilon$, the mean contributions are plotted as solid symbols and the fluctuating contributions are plotted as open symbols. The solid and dashed lines (and the corresponding colours) are the mean and fluctuating contributions for RBC (cf. [3]).

For the rate of change of background potential energy in VC, we obtain

$$\frac{\mathrm{d}E_b}{\mathrm{d}t} = -\Phi_{b2} + \Phi_d, \tag{14}$$

where

$$\Phi_{b2} = -\frac{\kappa g}{\rho_0 V}\oint_S (x_*\partial_i\rho)\cdot\hat{\mathbf{n}}\,\mathrm{d}S = \frac{\kappa g}{\rho_0}\left(\frac{L_x}{L_z}\right)\langle\partial_x\rho\rangle_{A(x,y,0)}, \tag{15}$$

$$\Phi_d = -\kappa g(\rho_0)^{-1}\left\langle(\mathrm{d}x_*/\mathrm{d}\rho)\,(\partial_i\rho)^2\right\rangle_V, \tag{16}$$

following the steps outlined in § 4 of [10]. We note that a third term is present in the equation derived by [10] (referred to as $S_{adv}$ the rate of change of $E_b$ due to advective mass across the bounding surface $S$) but since it is equal to zero in VC, we do not show this term in equation (14). $\Phi_{b2}$ is the buoyancy forcing rate. In VC, $\Phi_{b2}$ is equal to the rate of supply of horizontal heat flux at the vertical walls, which maintains the density field away from its minimum potential energy state. $\Phi_d$ is the rate of irreversible mixing. Since there is no net heating of the volume in VC, $\mathrm{d}E_b/\mathrm{d}t = 0$ and so $\Phi_{b2} = \Phi_d$, which is similar to RBC.

The rate of change of $E_a$ can then be obtained by subtracting equation (7) and equation (14):

$$\frac{\mathrm{d}E_a}{\mathrm{d}t} = \frac{\mathrm{d}E_p}{\mathrm{d}t} - \frac{\mathrm{d}E_b}{\mathrm{d}t} = \Phi_{a1} + \Phi_x - (-\Phi_{b2} + \Phi_d). \tag{17}$$

Thus, the mechanical energy exchange framework for VC can be formed by relating terms on the right-hand side of equations (6), (14) and (17). Figure 4(*a*) illustrates the framework and figure 4(*c*) shows the exchange rates for $\Phi_x$, $\varepsilon$ and $\Phi_{a1}$, all normalised by $\Phi_{b2}$. Since $\mathrm{d}E_p/\mathrm{d}t = 0$ (no net heating) and $\mathrm{d}E_k/\mathrm{d}t = 0$, therefore from equations (6) and (7), we find that $\Phi_{a1} = -\Phi_x$ and $-\Phi_x = \varepsilon$, which agree with the trends in figure 4(*c*). In addition, since $\mathrm{d}E_b/\mathrm{d}t = 0$, then $-\Phi_{b2} = \Phi_d$ which implies that the rate at which $E_a$ is generated in equation (14) (and also the rate of irreversible mixing) is directly proportional to the rate of energy exchange via buoyancy flux and rate of dissipation in VC.

## Mean and turbulent form

It is more informative to analyse the mean and turbulent-fluctuation contributions of the terms in figure 4(*a*). This is achieved by decomposing the kinetic and potential energies into the mean and turbulent contributions. Following [3], we obtain

$$\frac{\mathrm{d}\overline{E_k}}{\mathrm{d}t} = -\Phi_T - \overline{\Phi_x} - \overline{\varepsilon}, \tag{18}$$

$$\frac{\mathrm{d}E'_k}{\mathrm{d}t} = \Phi_T - \Phi'_x - \varepsilon', \tag{19}$$

$$\frac{\mathrm{d}E_a}{\mathrm{d}t} = \overline{\Phi_{a1}} + \Phi'_{a1} + \overline{\Phi_x} + \Phi'_x - (-\Phi_{b2} + \Phi_d), \tag{20}$$

where

$$\Phi_T = -\rho_0\langle\partial_j\overline{u_i}\,\overline{u'_iu'_j}\rangle_V, \tag{21}$$

the shear production term which quantifies the rate at which energy is converted from the mean flow to turbulence,

$$\overline{\Phi_x} = g\langle\overline{\rho}\,\overline{u}\rangle_V, \quad \Phi'_x = g\langle\rho'u'\rangle_V, \tag{22}$$

the energy conversions by the mean and turbulent buoyancy flux,

$$\overline{\varepsilon} = \nu\langle(\partial_j\overline{u_i})^2\rangle_V, \quad \varepsilon' = \nu\langle\overline{(\partial_j u'_i)^2}\rangle_V, \tag{23}$$

the mean and turbulent rate of dissipations,

$$\overline{\Phi_{a1}} = -g\langle\overline{\rho}\,\overline{u}\rangle_{A(L_x,y,z)}, \quad \Phi'_{a1} = -g\langle\rho'u'\rangle_{A(L_x,y,z)}. \tag{24}$$

the area-averaged mean and turbulent buoyancy flux at the top of the domain. Using equations (18)–(20), the framework in figure 4(*a*) is extended to include the mean and turbulent contributions as well as $\Phi_T$, and this is shown in figure 4(*b*).

In figure 4(*d*), we plot the relative contributions of the energy conversion rates from the mean and turbulent terms in equations (21)–(23) for VC (circular symbols) and compared the contributions with the relative contributions for RBC (solid and dashed lines of the same color). Similar to figure 4(*c*), all quantities are normalised by $\Phi_{b2}$. For VC, we find that the conversions from the mean contributions of the vertical buoyancy flux $-\overline{\Phi_x}$ increase from approximately 50% to a maximum of 80%. The increasing trend of $-\overline{\Phi_x}$ is matched by an increase in the conversions for turbulence production $\Phi_T$ (from approximately 25% to 60%) and a decrease in dissipation rates from mean velocities $\overline{\varepsilon}$ (from approximately 20% to 10%). As $\Phi_T$ increases with increasing *Ra*, the corresponding turbulent kinetic energy $\varepsilon'$ is increasingly dissipated and at $Ra = 10^9$ is approximately 90% of $\Phi_{b2}$. When compared to the relative contributions from RBC [3], the trends of $-\overline{\Phi_x}$ and $-\Phi'_x$ appear comparable at $10^7 \lesssim Ra \lesssim 10^8$. However, at matched *Ra* values, the contributions from both $\Phi_T$ and $\varepsilon'$ are higher for VC than for RBC, which suggests that small-scale turbulence is generated at much lower *Ra* in VC compared to RBC. The higher contributions from both $\Phi_T$ and $\varepsilon'$ in VC are commensurate with lower contributions from $\overline{\varepsilon}$.

### Mixing Efficiency

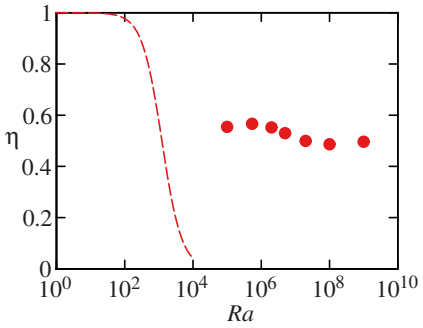


Figure 5: Mixing efficiency for VC using equation (25), where the dashed line is the laminar result and the symbols are the DNS results.

We quantify the mixing efficiency in VC following the definition used in [8] and [4]:

$$\eta = \frac{\Phi_d - \Phi_i}{\Phi_d - \Phi_i + \varepsilon}, \tag{25}$$

which measures the proportion of kinetic energy that is irreversibly converted to the background potential energy due to mixing [9]. Unlike in RBC where $\eta = 0.5(1 + Nu^{-1})$ [4], the mixing efficiency for VC cannot be written explicitly in terms of *Nu* because $\varepsilon$, which contains the vertical buoyancy flux term, is unclosed for VC [7]. In addition, $\Phi_i = 0$ for VC because of the periodic boundary condition imposed in the streamwise *x*-direction. For VC, we find that on average $\eta \approx 0.53$ (see figure 5) which is close to $\eta = 0.5$ expected for RBC [3]. This similarity of the values of $\eta$ could be attributed to the fact that in both VC and RBC, $\Phi_d \sim \varepsilon$ and in the case of RBC, $\Phi_i$ is negligible [3]. For comparison, we plot the laminar mixing efficiency value in figure 5. From the trend of the laminar mixing efficiency, we find a negligible contribution from the dissipation rate at low *Ra* ($\eta \approx 1$) which increasingly dominates at $10^2 \lesssim Ra \lesssim 10^4$ ($\eta \to 0$). However, we note that the latter result is presumably amenable to transitional flow dynamics, as indicated by the discontinuity in the laminar-to-turbulent $\langle E_k \rangle_t$ trend in figure 3.

### Conclusions

We investigate the conversion rates between potential energy and kinetic energy using the mechanical energy framework for VC for *Ra* ranging between $10^5$ to $10^9$ and $Pr = 0.709$. Using the framework, we compared the conversion rates in VC with that for RBC. The conversion rates for vertical buoyancy flux are similar in both VC and RBC at matched *Ra*. However, the turbulent production rate as well as the turbulent dissipation rate is higher in VC than for RBC (figure 4*d*), which suggests that small-scale turbulence is generated at a lower *Ra* in VC compared to RBC. The increased production of small-scale turbulence is commensurate with decreased dissipation rate of the mean motions. Since the heating and cooling in VC is uniquely restricted to the vertical walls, the rate of generation of available potential energy is directly proportional to the dissipation rate of kinetic energy (figure 4*c*). This relation is consistent with the value of mixing efficiency for VC, defined as the proportion of kinetic energy consumed by irreversible mixing, which is approximately 0.53 (figure 5). This value is also close to the value of mixing efficiency of 0.5 predicted for RBC.


### Acknowledgements

The authors thank the NCI National Facility in Canberra Australia and the Pawsey Supercomputing Centre for providing computing time.


### References


[1] Ahlers, G., Grossmann, S. and Lohse, D., Heat transfer and large scale dynamics in turbulent Rayleigh–Bénard convection, *Rev. Mod. Phys.*, **81**, 2009, 503–537.

[2] Gayen, B., Griffiths, R. W., Hughes, G. O. and Saenz, J. A., Energetics of horizontal convection, *J. Fluid Mech.*, **716**, 2013, R10.

[3] Gayen, B., Hughes, G. O., Griffiths, R. W., Gayen, B., Hughes, G. O. and Griffiths, R. W., Completing the mechanical energy pathways in turbulent Rayleigh–Bénard convection, *Phys. Rev. Lett.*, **111**, 2013, 124301.

[4] Hughes, G. O., Gayen, B. and Griffiths, R. W., Available potential energy in Rayleigh–Bénard convection, *J. Fluid Mech.*, **729**, 2013, R3.

[5] Hughes, G. O. and Griffiths, R. W., Horizontal convection, *Annu. Rev. Fluid Mech.*, **40**, 2008, 185–208.

[6] Lorenz, E. N., Available potential energy and the maintenance of the general circulation, *Tellus*, **7**, 1955, 157–167.

[7] Ng, C. S., Ooi, A., Lohse, D. and Chung, D., Vertical natural convection: application of the unifying theory of thermal convection, *J. Fluid Mech.*, **764**, 2015, 349–361.

[8] Peltier, W. and Caulfield, C., Mixing efficiency in stratified shear flows, *Annu. Rev. Fluid Mech.*, **35**, 2003, 135–167.

[9] Tseng, Y.-h. and Ferziger, J. H., Mixing and available potential energy in stratified flows, *Phys. Fluids*, **13**, 2001, 1281–1293.

[10] Winters, K. B., Lombard, P. N., Riley, J. J. and D'Asaro, E. A., Available potential energy and mixing in density-stratified fluids, *J. Fluid Mech.*, **289**, 1995, 115–128.